Lack of Telopeptides in Fibrillar Collagen I Promotes the Invasion of a Metastatic Breast Tumor Cell Line

Zoe N. Demou,[1] Michael Awad,[1] Trevor McKee,[1,2] Jean Yannis Perentes,[1,3] Xiaoye Wang,[1] Lance L. Munn,[1] Rakesh K. Jain,[1] and Yves Boucher[1]

[1]Steele Laboratory for Tumor Biology, Department of Radiation Oncology, Harvard Medical School and Massachusetts General Hospital, Boston, Massachusetts; [2]Biological Engineering Division, Massachusetts Institute of Technology, Cambridge, Massachusetts; and [3]Department of Thoracic Surgery, University Hospital of Lausanne (Centre Hospitalier Universitaire Vaudois), Lausanne, Switzerland

Abstract

Defective fibrillar collagen polymerization in primary tumors has been correlated with increased metastasis. However, it is unclear how collagen organization influences tumor invasion. In this study, we show that collagen I polymerized without telopeptides (the flanking regions of collagen molecules) can differentially affect the three-dimensional migration of mammary carcinoma cells. MDA-MB-231 cells capable of proteolytic degradation and mesenchymal motion, invaded telopeptide-intact and telopeptide-free collagen gels to the same extent. In contrast, MDA-MB-435S cells, with typical features of amoeboid cells (poor collagenolytic activity, rounded cell morphology), were 5-fold more invasive in telopeptide-free than telopeptide-intact collagen. A fraction of the MDA-MB-435S cells that invaded telopeptide-intact or telopeptide-free collagen had a rounded morphology; however, in telopeptide-free collagen, a significant fraction of the cells switched from a rounded to elongated morphology (protrusion formation). The dynamic changes in cellular shape facilitated MDA-MB-435S locomotion through the narrow interfiber gaps, which were smaller than cell diameters. Based on the spherical morphology of MDA-MB-435S cells, we tested if the changes in cell shape and invasion were related to RhoA-ROCK activity; GTP-bound RhoA was measured in pull-down assays. RhoA activity was 1.8-fold higher for MDA-MB-435S cells seeded on telopeptide-free than telopeptide-intact collagen. Y27632 inhibition of ROCK, a Rho effector, significantly reduced the changes in cellular morphodynamics and the invasion of MDA-MB-435S cells but did not alter the invasion of MDA-MB-231 cells. Thus, the higher RhoA activity of MDA-MB-435S cells in telopeptide-free collagen enhances the changes in cellular morphodynamics associated with motility and invasion. (Cancer Res 2005; 65(13): 5674-82)

Introduction

Tumor cell invasion is dependent on tumor-host interactions regulating a spectrum of cellular processes such as adhesion, survival, migration, as well as organization, proteolysis, and remodeling of the extracellular matrix (ECM; refs. 1, 2). During their passage through the ECM, tumor cells migrate individually by amoeboid or mesenchymal motion, or collectively as groups or sheets (3). Cells with a mesenchymal phenotype have a spindle-like shape and interact dynamically with collagen fibers, or other ECM molecules, via cellular receptors (e.g., integrins) and proteinases that remodel the matrix (3, 4). Local proteolysis by matrix metalloproteinases, or enzymes from the urokinase plasminogen activation cascade, has been associated with enhanced invasion and migration in collagen gels (5–7). Certain mammalian cells such as infiltrating leukocytes and invading neoplastic cells in tumors, or *in vitro* inside collagen gels or matrigel, migrate employing an amoeba-like mechanism. Amoeboid movement is generated via changes in cell shape. In this case, mostly round cells undergo dynamic extension and retraction of pseudopods to advance through the matrix without significant integrin-mediated contacts and with limited degradation or remodeling of their microenvironment (3, 8). Furthermore, tumor cells can adapt to their microenvironment and adopt appropriate shape, cell matrix affinity, and mode of locomotion. For example, cells can switch from mesenchymal to amoeboid migration in the presence of protease inhibitors (9). However, the exact causes that determine the preferred mechanism of locomotion and the variables that modulate the efficiency of tumor cells invading the tumor microenvironment have not been fully characterized yet.

Fibrillar collagen I, the major ECM component of most normal tissues and tumors, provides structural organization and mechanical strength. The collagen I molecule is a triple helix of two α1 chains and one α2 chain, which are flanked by nonhelical NH_2- and COOH-telopeptide regions (telopeptides). Collagen molecules can aggregate spontaneously into fibrils by staggering in an overlapping fashion with their neighbors. The telopeptides are not essential for fibril formation (10); however, they form intramolecular and intermolecular cross-links that promote the staggered pattern and enhance the tensile strength of fibrillar collagen (11–13). Cross-link formation is catalyzed by the enzyme lysyl oxidase (14, 15).

Recent studies have suggested that collagen I plays a significant role during tumor cell invasion and metastasis. The overexpression of the α1 and α2 collagen I genes is part of a 17-gene signature associated with increased metastasis and poor clinical outcome in patients with primary prostate, breast, and lung cancers (16). Additionally, the presence of fibrotic foci (composed of proliferative fibroblasts) in invasive human breast carcinomas have been associated with a greater metastatic potential (17). In normal tissues, the cross-links formed by collagen I telopeptides are fully matured, whereas defects in collagen polymerization have been reported in breast and ovarian carcinomas. The presence of disorganized collagen bundles, in invasive breast carcinoma and ovarian tumors, has been linked to reduced levels of telopeptide cross-links (18, 19). The abnormal collagen organization in tumors could result from reduced expression of lysyl oxidase (20) and/or

Note: Supplementary data for this article are available at Cancer Research Online (http://cancerres.aacrjournals.org/).

Requests for reprints: Yves Boucher, Department of Radiation Oncology, COX-7, Massachusetts General Hospital, 100 Blossom Street, Boston, MA 02114. Phone: 617-726-4082; Fax: 617-726-3603; E-mail: yves@steele.mgh.harvard.edu.

telopeptide degradation by matrix metalloproteinases (21–23), or aspartyl proteases (24, 25). Furthermore, the high levels of collagen telopeptides in the serum of breast and ovarian cancer patients were prognostic of bone metastasis and decreased survival (26–28).

Therefore, the lack of telopeptides and the subsequent changes in fibrillar collagen organization could enhance tumor cell migration and invasion. To test this hypothesis, we quantified the invasion of two metastatic mammary carcinoma cell lines into collagen I gels with intact and degraded telopeptides. To explain the differences in percent invasion and penetration depth, we assessed the collagenolytic activity, RhoA activity, cellular adhesion and shape, speed of cell locomotion, and the organization, spacing, and stiffness of the collagen I lattice.

Materials and Methods

Cell culture. The invasive mammary carcinoma cell lines MDA-MB-231 and MDA-MB-435S were obtained from the American Type Culture Collection (Manassas, VA). The cells were cultured in DMEM supplemented with 1% penicillin/streptomycin (P/S) and 10% fetal bovine serum (FBS) in a humidified 5% CO_2 incubator. For all functional assays, the cells were detached through brief contact with trypsin-EDTA and were resuspended in DMEM supplemented with 0.5% FBS and 1% P/S (invasion medium).

Collagen type I stock solutions. We used two different sources of collagen, native telopeptide-intact collagen I extracted from rat tail tendon in acetic acid (BD Biosciences, San Jose, CA) and telopeptide-free collagen, Vitrogen (Cohesion Technologies, Palo Alto, CA), a pepsin-solubilized collagen from bovine skin. Rat tail collagen consists of 95% to 99% collagen I, whereas Vitrogen is 99.9% pure collagen with 95% to 98% collagen I, the remainder being collagen III. Furthermore, control experiments were done with (i) purified telopeptide-intact collagen from the original telopeptide-intact collagen stock after purification with DEAE-cellulose (Sigma, St. Louis, MO) column chromatography and high-salt precipitation and (ii) pepsin-treated telopeptide-intact collagen produced from the original telopeptide-intact collagen stock after digestion with pepsin in a 10:1 ratio for 48 hours. The collagen was then dialyzed, neutralized, and purified by *in vitro* fibrillogenesis. The fibers were collected by centrifugation and were dissolved in acetic acid. The concentration of the customized collagen products was measured with the Sircoll assay (Biocolor, Westbury, NY).

Preparation of collagen gels for functional assays. Aliquots of the collagen stock solutions were diluted (2 mg/mL) with invasion medium and PBS (10×) and carefully adjusted to pH 7.4 with sterile NaOH (1 N). The collagen mixture was poured in multiwell culture plates (500 μL/well of a 24-well plate) for invasion and adhesion assays, RNA isolation, cell tracking, and second harmonic generation (SHG) imaging of the collagen gels with a multiphoton microscope. After collagen polymerization in a humidified incubator (5% CO_2) at 37°C, the gels were overlaid with medium and further cured overnight in the incubator before cell seeding. Cells were also mixed with the collagen mixture before polymerization to form cell-populated gels for cell tracking. To increase the stiffness of telopeptide-free collagen I, the polymerized collagen gels were treated with 100 mmol/L D(−) ribose (Sigma) in PBS for 5 days. Ribose treatment (15–30 mmol/L) of collagen I gels for 1 week[4] or collagen I tissue equivalents (29) increased their tensile strength. The gels were then washed thrice with PBS and thrice with medium before cell seeding.

SDS-PAGE. To test the purity, the collagen stock solutions were subjected to electrophoresis under nondenaturing conditions on 7.5% SDS-PAGE gels and stained with silver (Rapid Silver Staining Kit, Sigma). To analyze the degradation of collagen by MDA-MB-231 and MDA-MB-435S, cells were cultured on telopeptide-intact and telopeptide-free polymerized collagen I. The medium overlaying the cells was collected after 48 hours, concentrated, and SDS-PAGE gels were prepared and stained with Coomassie blue.

[4] N. Dubey and R. Tranquillo, personal communication.

RhoA activity. RhoA activity was measured with the Rho Activation Assay Biochem Kit (Cytoskeleton, Denver, CO). In brief, 2.5×10^6 cells were plated on telopeptide-intact and telopeptide-free collagen for 24 hours. Following cell lysis, the gels were scraped and the samples were cleared by ultracentrifugation (20,000 rpm, 15 minutes, 4°C) and concentrated using spin columns (Milipore Corp., Billerica, MA). RhoA activity was determined according to the manufacturer's protocol.

Inhibitor study. To distinguish the distinct migratory mechanisms of MDA-MB-231 and MDA-MB-435S cells in collagen gels, we quantified the invasion in the presence of Y27632, a Rho-kinase inhibitor (Calbiochem, San Diego, CA; ref. 30). More specifically, MDA-MB-231 and MDA-MB-435S cells resuspended in the invasion medium were seeded on top of the polymerized collagen gels and subsequently Y27632 (10 μmol/L) was added to the wells. Rho activity was inhibited by recombinant exoenzyme C3 transferase (10 μg/mL; Cytoskeleton, Denver, CO).

Quantification of cell invasion and adhesion. The percentage of invaded cells and invasion depth in collagen gels was measured with an aperture-shifting microscopic method (31) 96 hours after cell seeding. Cell adhesion was measured 1 and 3 hours after seeding. The gels were washed very gently thrice with PBS and images of the surface were acquired at 4× magnification.

Time-lapse image acquisition for measuring cell speed and cell morphology. Time-lapse imaging was done 1 day after seeding for cells seeded on top and for cells embedded in collagen gels. The gels were placed in a custom-made humidified microincubator, maintained at 37°C, and buffered with 5% CO_2 balance air. Images were acquired with 10× and 20× objectives via a custom-made automation in the Openlab software (Improvision, Lexington, MA), based on a previously published algorithm (32), every 30 minutes for 12 hours in adjacent XY fields of view and with a 10-μm step optical sectioning up to 200-μm depth.

To extract morphologic features, the outlines of the cells (on top and inside the gels) were manually traced on their focal plane and the images were thresholded. Then standard analysis tools of the ImageJ software (NIH, http://rsb.info.nih.gov/ij/) were applied to calculate the cell area (as a measure of cell matrix affinity) and the cell circularity (as a measure of cell elongation) from snapshots of cells throughout the gels. The "circularity" measurement tool fits an ellipse to the area corresponding to each individual cell trace and calculates the circularity as the ratio of the minor over the major axis of the fitted ellipse. Furthermore, each cell was individually observed during the recorded time-lapse movies and was characterized as "round" when it did not form any protrusions longer than half a cell body diameter at any time point during the tracking period. Likewise, cells "with protrusions" formed at least one protrusion longer than the above threshold during the tracking period. "Motile" cells shifted the center of their body from their initial position at time zero (onset of tracking) for a distance at least a quarter of the length of one main body diameter, at least once during the tracking period. The cell speed was calculated as the net cell translocation over the total time of image acquisition.

Multiphoton laser scanning microscopy and collagen gel imaging with second harmonic generation. SHG imaging was done in gels cured overnight with invasion medium or 1 day after seeding. Cells cultured on collagen gels were washed twice with PBS and stained for 20 minutes with 0.5 μg/mL calcein AM (Molecular Probes, Eugene, OR) in serum-free DMEM. Before imaging, gels were washed twice with PBS and were overlaid with invasion medium. Cells and SHG of collagen fibers were imaged with a custom-built multiphoton laser scanning microscope as described previously (33). Fluorescence and second harmonic signal were generated at the sample, collected every 2-μm step size by a 0.9 NA water immersion lens (either ×20 or ×63, Achroplan, Zeiss, Thornwood, NY), and separated from 870-nm input excitation light (Ti-Sapphire laser, SpectraPhysics, Mountain View, CA) by a long-pass dichroic filter (690/DRLP). The SHG signal was reflected off a second long-pass dichroic filter (4754/DRLP) and collected with a 435DF40 emission filter (Chroma Technology, Brattleboro, VT), whereas the calcein signal was passed through the second dichroic and collected by a 525DF100 emission filter into HC125-02 Photomultiplier tubes (Hamamatsu, Bridgewater, NJ).

Pore analysis in collagen gels. Pore characteristics such as cross-sectional areas, interfiber distances, and vertical pore lengths (depths) were measured from the SHG optical sections for telopeptide-intact, telopeptide-free, and ribose-treated telopeptide-free collagen lattices. More specifically, an individual z-section in the middle of a gel was chosen for analysis, within which a cohort of individual pores were outlined manually and their corresponding areas were calculated. Adjacent z-sections were then searched in the vicinity of the measured section to find the most proximal planes above and below at which fibers would cross the projected pore area. The distance from a section showing a fiber crossing below the pore to a fiber crossing above the pore was measured. This distance is indicative of the vertical length of the pore and was called "pore depth" (obviously, this method underestimates the actual length of the three-dimensional pore when the pore deviates horizontally). Additionally, interfiber spacing was measured using a technique similar to that described by Friedl et al. (34). Vertical sections corresponding to planes perpendicular to the surface of the gel were created from the optical z-sections using the "RESLICE" command in ImageJ software. These sections were then used to measure the nearest neighbor interfiber spacing for a cohort of collagen fibers in telopeptide-intact, telopeptide-free, and ribose-treated telopeptide-free collagen.

Statistics. All measured variables were extracted from at least three independent experiments. Results are presented as percentile plots, or as mean values ± SD. Significance was determined by a *t* test or ANOVA with Tukey's post hoc test for paired comparisons. Analysis of nonparametric data was done with the Mann-Whitney test. The symbol "*" in the figures indicates $P < 0.05$.

Results

To assess the role of collagen telopeptides in tumor cell invasion, we initially compared the invasion of MDA-MB-231 and MDA-MB-435S breast carcinoma cell lines in telopeptide-intact (native) and telopeptide-free (pepsin-solubilized, Vitrogen) collagen I. MDA-MB-231 cells invaded telopeptide-intact and telopeptide-free collagen gels to the same extent. In contrast, there was a 5-fold greater invasion of MDA-MB-435S cells in telopeptide-free than telopeptide-intact collagen I (Fig. 1*A*) indicating that the presence of telopeptides inhibits the migration of MDA-MB-435S cells in collagen I gels. These results were consistent with invasion measurements in telopeptide-intact native collagen degraded with pepsin, where MDA-MB-435S cells exhibited a 4.0-fold greater invasion compared with nonsolubilized native collagen (Fig. 1*B*). The depth of invasion of MDA-MB-435S cells was also significantly less in native telopeptide-intact collagen compared with pepsin-solubilized native and Vitrogen collagen (Fig. 1*C*). Furthermore, to test the possibility that small amounts of noncollagenous molecules (e.g., proteoglycans) present in native collagen might be responsible for the differential invasion of MDA-MB-435S cells, we measured their invasion in native collagen purified by DEAE-cellulose chromatography and salt precipitation. The invasion of MDA-MB-435S cells was 1.6-fold higher in purified than in nonpurified native collagen. However, MDA-MB-435S invasion was still 2.3-fold higher in telopeptide-free collagen that in purified collagen I (Fig. 1*B*). Silver staining of SDS-PAGE gels of native collagen I revealed two faint bands, at ~46,000 and 65,000 in MW, in addition to the typical β, α1, and α2 bands of collagen I. The 46,000 and 65,000 bands were not observed in SDS-PAGE gels of Vitrogen or purified native collagen

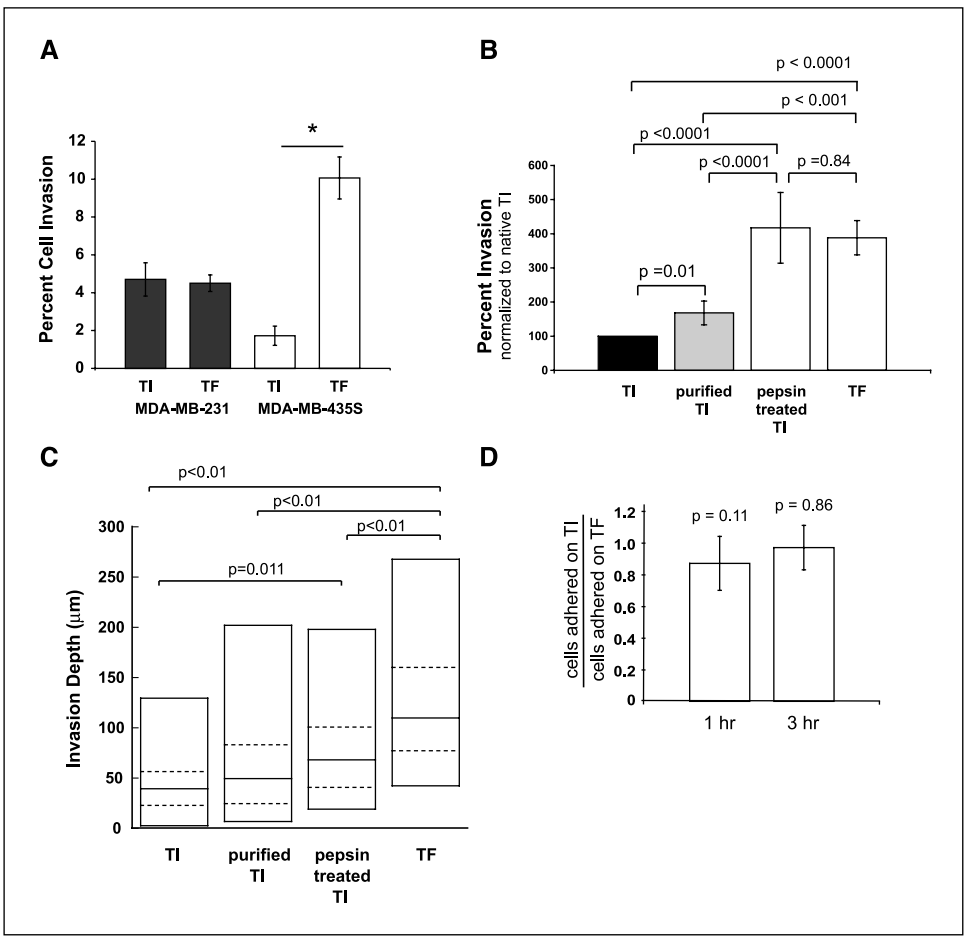

Figure 1. *A,* percent invasion of MDA-MB-231 and MDA-MB-435S cells in rat tail telopeptide-intact (*TI*) and bovine skin (Vitrogen) telopeptide-free (*TF*), collagen I gels. In four days, MDA-MB-231 cells invaded telopeptide-intact and telopeptide-free collagen gels to the same extent. During the same time period, there was a 5-fold greater invasion of MDA-MB-435S cells in telopeptide-free than telopeptide-intact collagen I gels. *B,* MDA-MB-435S cell invasion plotted as percentage of the invasion in native rat tail telopeptide-intact collagen for (i) purified rat tail telopeptide-intact, (ii) pepsin-treated rat-tail telopeptide-intact, and (iii) Vitrogen telopeptide-free. *Columns,* mean ($n = 3$); *bars,* SD. *C,* the corresponding invasion depth percentile plot. The horizontal lines in (*C*) show the 10th, 25th, 50th (median), 75th, and 90th percentile for the pooled data of three independent experiments. In telopeptide-intact, the cells were mostly located within 40 μm from the gel surface. The invasion in pepsin-solubilized collagen (telopeptide free and pepsin-treated telopeptide intact) was significantly deeper. *D,* number of MDA-MB-435S cells which adhered to rat tail telopeptide-intact versus Vitrogen telopeptide-free collagen gels 1 and 3 hours after seeding. There is no preferential cellular adhesion on telopeptide-intact compared with telopeptide-free collagen ($n = 3$).

I (data not shown). Furthermore, cell attachment on telopeptide-intact and telopeptide-free collagen (Fig. 1*D*) was comparable excluding an effect of cell matrix adhesion in the differential invasion of MDA-MB-435S cells.

To determine whether the difference in invasion between the two cell lines was related to collagen degradation, the medium overlaying cells cultured on top of collagen gels was analyzed by SDS-PAGE. The electrophoresis results indicate that MDA-MB-231 degraded the β and α bands of telopeptide-free and telopeptide-intact collagen to a greater extent than MDA-MB-435S cells (Fig. 2*A-B*). To compare the collagen degradation induced by tumor cells, the intensity of the bands from the medium with cells were measured and normalized to the intensity of the bands from the medium without cells. The fractional band intensities (lumped results of β and α bands) for telopeptide-intact and telopeptide-free collagen were 28% and 42% for MDA-MB-231 and 58% and 66% for MDA-MB-435S, respectively. Degradation products of collagen (lower bands on SDS-PAGE gels) were present in the medium of MDA-MB-435S and MDA-MB-231 cells and absent from the medium not seeded with cells (control). The intensity of the degraded bands was 1.7-fold (telopeptide-free collagen) and 1.75-fold (telopeptide-intact collagen) higher in the medium of MDA-MB-231 than MDA-MB-435S cells. The SDS-PAGE analysis suggests that matrix degradation is not the cause of the higher invasion of MDA-MB-435S in telopeptide-free than telopeptide-intact collagen.

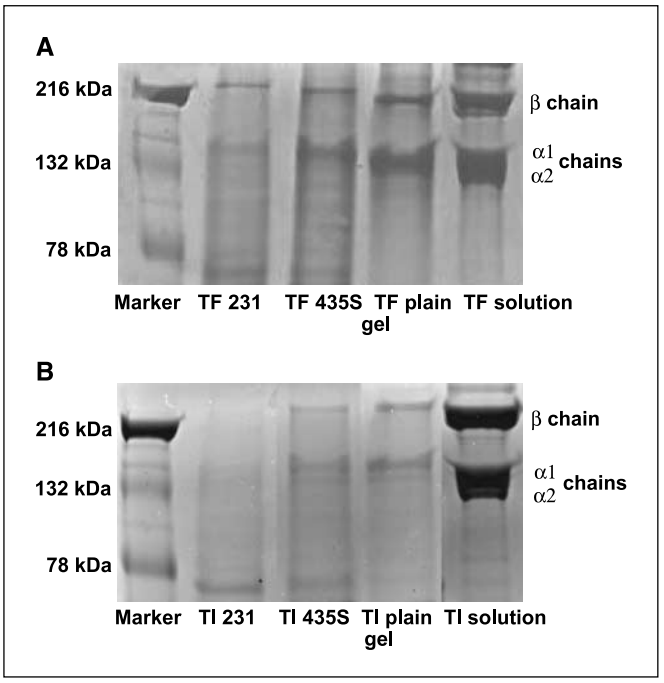

Figure 2. SDS-PAGE gel for medium overlaying (*A*) telopeptide-free (*TF*) and (*B*) telopeptide-intact (*TI*) collagen I gels plated with MDA-MB-231 and MDA-MB-435S cells, for telopeptide-intact and telopeptide-free gels without cells, and for nonpolymerized soluble telopeptide-intact and telopeptide-free collagen. As seen by the lower intensity of the α and β bands in comparison with the plain gels without cells, MDA-MB231 cells degraded the telopeptide-intact and telopeptide-free collagen liberated in the culture medium to a great extent. In comparison with MDA-MB-231, the MDA-MB-435S cells had a lower collagenolytic activity, and there was no obvious difference in α and β band intensity for telopeptide-intact and telopeptide-free collagen seeded with MDA-MB-435S cells. Some of the degradation products of collagen can be seen below the 78 daltons marker; note that the intensity of the bands is higher for the MDA-MB-231 than MDA-MB-435S cells.

Because cell adhesion and matrix degradation could not explain the differential invasion of MDA-MB-435S in telopeptide-intact versus telopeptide-free collagen, we studied whether the morphology of MDA-MB-435S cells was modulated by the lack or presence of telopeptides in polymerized collagen I gels. Most MDA-MB-231 cells had a spindle shape on the surface and inside both telopeptide-free and telopeptide-intact collagen I gels. In contrast, MDA-MB-435S cells were either round or switched from a rounded to elongated shape due to protrusion formation (Fig. 3*A-C*). MDA-MB-435S cells could form and retract short protrusions before establishing longer and thicker protrusions (Fig. 3*C*; Supplementary Movie 1). The retraction and formation of new protrusions could occur at least as fast as every 30 minutes (time-lapse interval). In both types of gels, MDA-MB-435S cells showed a rounded motility (Supplementary Movie 2). In comparison with telopeptide-intact collagen, cells in telopeptide-free collagen could often follow the lead of longer protrusions (Supplementary Movie 1). Cells contacting telopeptide-intact collagen were more quiescent morphologically. Protrusions formed by MDA-MB-435S cells were in telopeptide-intact more often than in telopeptide-free collagen, quite long (up to six body lengths in some cases), thin, and static, often maintaining their length and thickness for at least 12 hours (Fig. 3*D*). This type of protrusion did not promote the migration of MDA-MB-435S cells in either telopeptide-intact or telopeptide-free collagen. Thus, dynamic changes in cell shape are facilitated in telopeptide-free collagen.

Interestingly, the shape and size of MDA-MB-435S cells varied between the top and inside telopeptide-free collagen gels. Cell circularity and area measurements showed that the cells were mostly round on top and significantly more elongated and spread inside telopeptide-free collagen (Fig. 4*A*; Supplementary 3A). As for telopeptide-intact collagen, the MDA-MB-435S cells were mostly spherical; there was no difference in cell circularity or surface area between cells on top or inside the gel.

Quantification of cell morphology in three-dimensional showed that over 70% of MDA-MB-435S cells were round in contact with telopeptide-intact, whereas a significantly smaller percentage (about 50%) of the cells were round in telopeptide-free collagen (Fig. 4*B*). During the tracking period of 12 hours, in telopeptide-intact collagen only about 30% of the cells moved more than one cell diameter. More specifically, cells capable of such displacement were one third of the round cells and one third of cells with protrusions in telopeptide-intact collagen (Fig. 4*B*). About 50% of the cells could move more than one cell diameter in telopeptide-free collagen, with 40% of the round cells and 60% of cells with protrusions moving by more than one cell diameter. Cells with protrusions were 3-fold more likely to migrate in telopeptide-free than telopeptide-intact collagen (Fig. 4*B*).

The average cell speeds calculated for MDA-MB-435S cells embedded in three-dimensional gels were similar in telopeptide-intact (0.017 ± 0.0189 μm/min) and telopeptide-free (0.0185 ± 0.0187 μm/min) collagen. However, in telopeptide-intact collagen a significant fraction of the cells were immobile over the tracking period of 10 hours (Supplementary Movie 2), whereas in telopeptide-free collagen there was a net displacement of every cell. To represent this difference in motility, the cutoff for immobile cells was set at less than a quarter of a cell diameter. Figure 4 shows the significantly lower fraction of immobile cells in telopeptide-intact collagen and the percentage of cells that moved by a quarter to one cell diameter was significantly higher in telopeptide-free gels. Over the 10-hour period, only a minor

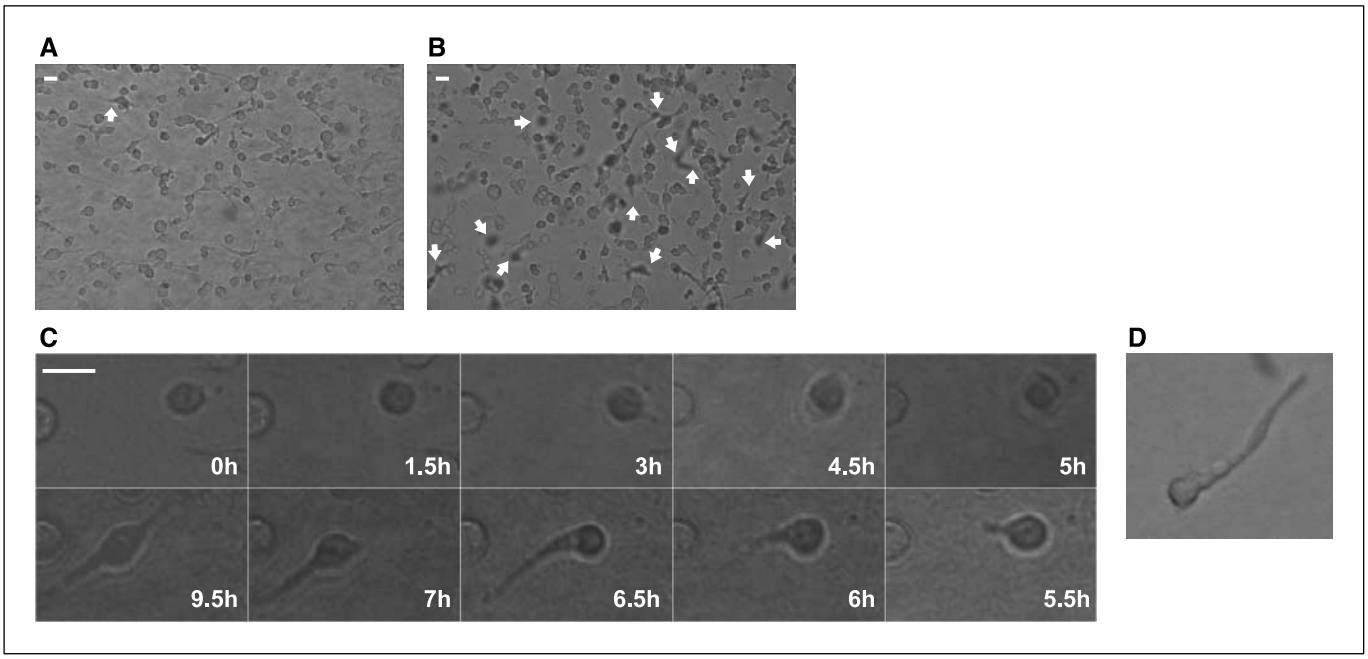

Figure 3. Snapshot (10×) of the surface of (*A*) telopeptide-intact (*TI*) and (*B*) telopeptide-free (*TF*) collagen gels 4 days after the seeding of MDA-MB-435S cells. Cells on top of both gels are mostly round. There is a greater number of cells (*arrows*) invading telopeptide-free than telopeptide-intact gels. *C,* time lapse of MDA-MB-435S migration in telopeptide-free collagen. At early time points (0-5.5 hours), there is little net displacement of the cell, which tumbles in place and forms protrusions in different directions. Then between 6.5 and 9.5 hours, the cell moves in the direction of a large protrusion (see also Supplementary Movie 1). *D,* protrusions formed by MDA-MB-435S cells on telopeptide-intact gels are often very long, thin and they do not promote cell migration. Bars, 20 μm.

fraction of the cells were capable of larger displacements in either gel type (Fig. 4*C*). The cell speeds on top of the gel were slightly faster than inside the gel and no difference in cell speed was found between telopeptide-intact and telopeptide-free gels (mean speed, 0.02 μm/min).

The relatively round shape and limited proteolysis suggested that MDA-MB-435S used amoeboid motions to invade collagen I gels. For some cancer cells, amoeboid movement in three-dimensional substrates is known to be promoted by RhoA signaling through Rho-kinase (ROCK; ref. 30). To determine if RhoA activity was associated with differences in tumor cell invasion, MDA-MB-435s cells were seeded on telopeptide-intact and telopeptide-free collagen I for 24 hours and RhoA activity was measured in cellular extracts. The RhoA activity was 1.8-fold higher for MDA-MB-435S cells interacting with telopeptide-free than telopeptide-intact collagen gels (Fig. 5*A*). To further substantiate the role of Rho-ROCK signaling, we did invasion experiments with Y27632, a ROCK inhibitor. Y27632 significantly reduced the invasion and formation of protrusions (increased cell circularity) by MDA-MB-435S cells in telopeptide-free collagen (Fig. 5*B-E*). In contrast, Y27632 did not inhibit the invasion of MDA-MB-231 cells (Fig. 5*D*). The invasion of MDA-MB-435S cells in telopeptide-free collagen was also significantly reduced by C3 transferase inhibition of Rho (data not shown).

Based on the limited invasion and reduced formation of cellular protrusions, we speculated that the size of void spaces between fibers (pores), or collagen stiffness could influence the migration of MDA-MB-435S cells. SHG imaging showed that telopeptide-intact collagen is organized into a network of long and thick fibers, which are interconnected (Fig. 6*A*). Telopeptide-free collagen fibers were shorter, thinner, and more closely packed than in telopeptide-intact collagen (Fig. 6*B*). The measured pore area, interfiber spacing, and pore depth were significantly larger in telopeptide-intact than telopeptide-free gels (Fig. 6*F*; Supplementary 3B and C). For both telopeptide-intact and telopeptide-free collagen, the pore area and interfiber spacing were smaller than the diameter of MDA-MB-435S cells (Fig. 6*D* and *E*).

The smaller pore size in telopeptide-free collagen suggests that the increased invasion of MDA-MB-435S in telopeptide-free collagen is not related to the size of the void space between collagen fibers. Because the tensile strength of telopeptide-intact is higher than telopeptide-free collagen (12, 13), we tested if invasion was related to differences in collagen stiffness. Telopeptide-free collagen gels were artificially stiffened with ribose, which forms nonenzymatic cross-links in the collagen. Ribose treatment of telopeptide-free collagen significantly reduced the invasion of MDA-MB-435S by 50% and increased the average cell circularity (Fig. 6*G* and *H*). Based on SHG imaging, there were no differences in structural organization (Fig. 6*C*), average pore cross-sectional area, interfiber distance, and average pore depth between untreated and ribose-treated telopeptide-free collagen gels (Fig. 6*D*; Supplementary 3B and C). In addition, ribose treatment of telopeptide-free collagen or its interaction with serum did not modify cell adhesion (Supplementary 3D and E).

Discussion

Cell deformability, proteolytic degradation, matrix displacement, and matrix phagocytosis are critical factors in cell migration (4, 35, 36). Migrating cells adopt the most efficient mechanism that enables them to overcome the biological and mechanical resistances of the ECM. The flexibility to exploit any combination of the above mechanisms determines the invasiveness of a cell population. In the absence of efficient proteolysis,

three-dimensional tumor cell migration relies on amoeboid motions, as cells physically squeeze their way through the matrix. Our findings show that their advances, in this case, are facilitated by a mechanically compromised microenvironment.

Defects in telopeptide cross-link formation and collagen organization in primary tumors (19, 20) have been linked to metastasis and disease progression in patients with breast and ovarian cancer (26, 27). In addition, reduced expression of decorin and lumican, two small proteoglycans that provide tensile strength to fibrillar collagen, decreased survival in breast cancer patients (37). The abnormal collagen found in invasive breast carcinoma and other tumors has been associated with reduced telopeptide cross-links due to low expression of lysyl oxidase, or proteolytic degradation of the telopeptides (19, 20). Our results show that the lack of telopeptides in collagen I gels affects the organization of the lattice and can enhance the invasion of breast carcinoma cells depending on their mode of locomotion. MDA-MB-231 cells that degrade fibrillar collagen and have a high affinity for collagen I (spindle shape), equally invaded gels polymerized with or without telopeptides. MDA-MB-435S cells with a smaller collagenolytic activity invaded more in telopeptide-free than in telopeptide-intact collagen. The increased invasion of MDA-MB-435S cells in telopeptide-free collagen was facilitated largely by the plasticity of their shape and the dynamic formation of protrusions. In contrast, most MDA-MB-435S cells that invaded telopeptide-intact collagen were round with limited cellular shape change.

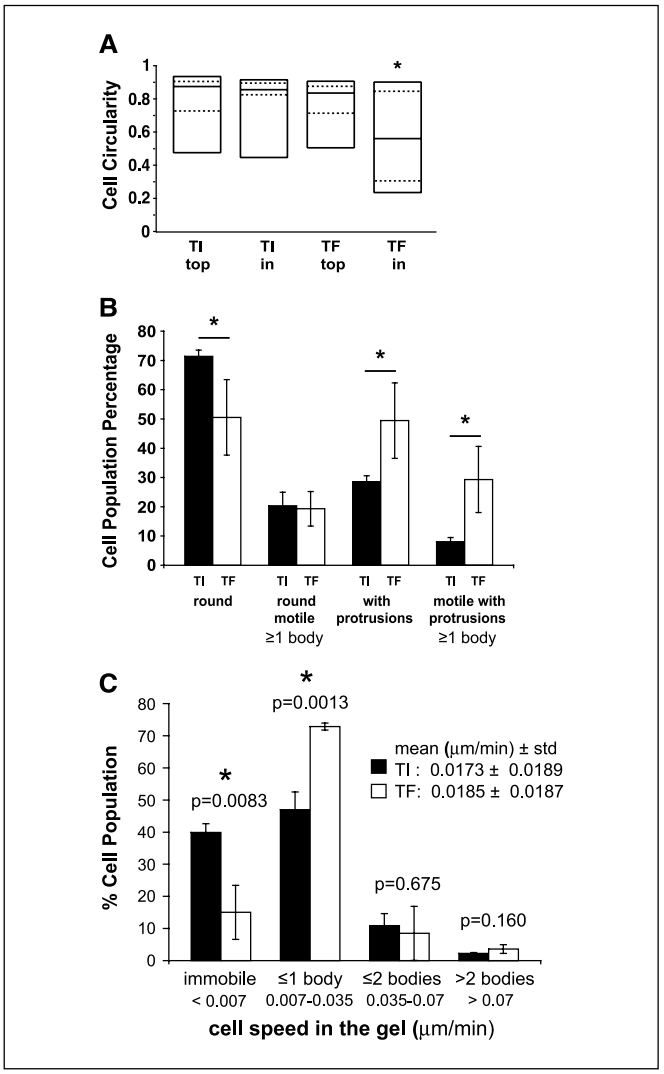

Figure 4. *A,* percentile plot of cell shape circularity for MDA-MB-435S cells on top and inside telopeptide-intact (*TI*) and telopeptide-free (*TF*) collagen. *B,* population percentages of MDA-MB-435S cells. The sum "round" plus "with protrusions" adds up to the total cell population (100%). The sum of "round motile" plus "motile with protrusions" represents the "total motile" population. *C,* histogram of the average speed of locomotion for cells embedded in telopeptide-intact and telopeptide-free collagen gels. There is no significant difference in mean average speeds; however, the percentage of immobile cells (moving less than a quarter of a cell body during 10 hours) is significantly higher in telopeptide-intact than telopeptide-free gels, whereas the percentage of cells capable of displacements up to one body size is significantly larger in telopeptide-free than telopeptide-intact gels. All plots represent three independent experiments with about 100 cells each per experiment.

Amoeboid movement though relatively simple mechanistically is a very effective mode of migration. Cells employ Rho signaling and recruitment of ROCK during cortical actin dynamics that generate contractile forces through weak adhesions to the substrate and allow for changes in cell shape and cell motility that are independent of pericellular proteolysis (30, 36). MDA-MB-435S cells exhibited typical features of amoeboid cells, such as (a) low affinity for collagen I, as seen by the mostly round cell shape and formation of cellular clusters on top of collagen gels; (b) dynamic protrusions and cell shape plasticity; (c) negligible collagenolytic activity; and (d) RhoA-ROCK-dependent migration (30). In both telopeptide-intact and telopeptide-free collagen, MDA-MB-435S cells had a rounded motility and in telopeptide-free collagen a significant fraction of MDA-MB-435s cells switched from a rounded to elongated morphology associated with cell movement. Inhibition of ROCK by Y27632 inhibited the transition from a rounded to elongated morphology (increased cell circularity, Fig. 5*E*). Thus, ROCK inhibition can reduce the movement of round tumor cells (30) and the motility of tumor cells that switch from rounded to elongated shapes.

The differential invasion of MDA-MB-435S cells in telopeptide-intact and telopeptide-free collagen was not related to differences in cellular affinity on top of the two collagen substrates. On both substrates, the adhesion, circularity, and speed of MDA-MB-435S cells were similar. Although MDA-MB-231 cells had a higher collagenolytic activity than MDA-MB-435S cells, there was no obvious difference in telopeptide-free and telopeptide-intact collagen degradation by MDA-MB-435S cells (Fig. 2). Furthermore, the broad-spectrum matrix metalloproteinase inhibitor, GM6001 did not influence the invasion of MDA-MB-435S cells (data not shown). Collagenolytic activity is probably not the cause of the differential invasion of MDA-MB-435S cells in the two collagen substrates.

Why are MDA-MB-435S cells more mobile and invasive in telopeptide-free than telopeptide-intact collagen I? The SHG imaging showed striking structural differences between telopeptide-intact and telopeptide-free collagen lattices. Telopeptide-free collagen polymerizes into a diffuse arrangement of short and thin fibers. On the other hand, native telopeptide-intact collagen forms a meshwork of thick, long, and interconnected fibers suggesting a structure with higher resistance to deformation. The tensile strength of collagen gels polymerized without telopeptides is known to be lower (12, 13), and artificial stiffening of telopeptide-free collagen gels with ribose inhibited migration, thus suggesting that MDA-MB-435S cells can locally deform or displace the three-dimensional substrate to increase the interfiber gap size. For example, lymphocytes can displace collagen fibers by 2 to 5 μm during their amoeboid motion (4, 38). The stiffness of

telopeptide-intact collagen, in lack of adequate collagenolysis, may limit cellular deformability and restricts invading cells to shallow depths (Fig. 1*C* and Fig. 4*A*). The cells cannot squeeze their way through the matrix and their invasion exploits proximal pores of appropriate size. The average spacing between fibers in telopeptide-free and telopeptide-intact collagen is significantly smaller than the size of cells therefore gaps that are wide and long enough to permit the movement of round cells are limited. The higher percentage and deeper invasion of MDA-MD-435S in telopeptide-free collagen may be facilitated in part by the enhanced plasticity of MDA-MB-435S cells, which formed dynamic protrusions and were able to squeeze through the lattice. Cells with protrusions were 3-fold more likely to be motile in telopeptide-free than telopeptide-intact collagen I (Fig. 4*B*). Because Rho-ROCK activity regulates change in cytoskeleton organization and cell shape, the higher RhoA activity in telopeptide-free than telopeptide-intact collagen suggest that the invasion of MDA-MB-435s cells is not only dependent on the interfiber spacing or collagen fiber deformability. Similar to telopeptide-intact collagen I, the ROCK inhibitor Y27632 significantly reduced the elongation of MDA-MB-435S cells (protrusion formation) and tumor cell invasion thus suggesting that the higher Rho-ROCK activity of MDA-MB-435S cells in telopeptide-free collagen promotes the changes in cellular morphology associated with migration and invasion through the narrow interfiber gaps.

RhoA and RhoC overexpression in tumor cells enhances invasion and metastasis formation (39–41). Similarly, the activation of the Rho effector ROCK leads to the dissemination of neoplastic cells in primary tumors (42) and the ROCK inhibitors, Y-27632 and Wf-536, inhibit the development of metastasis (43, 44). Thus, understanding the regulation of Rho activity by soluble factors and extracellular matrix molecules such as collagen I is significant. Similar to our findings, recent studies have shown that collagen I induces a significant activation of RhoA in colon and squamous carcinoma cells (45, 46). However, in contrast to our results with the invasion of MDA-MB-435S cells in telopeptide-free collagen, RhoA activation did not promote the invasion of squamous and colon carcinoma cells and the pharmacologic inhibition of RhoA or ROCK enhanced cell invasion. This differential effect of RhoA or ROCK inhibition on tumor cell invasion is most likely related to differences in cellular morphology and adhesion (e.g., focal adhesion formation). Sahai et al. (30) showed that RhoA inhibition by C3 transferase and ROCK by Y27632 reduced the invasion of rounded tumor cells in matrigel, whereas both inhibitors enhanced the invasion of elongated tumor cells. In the present study, Y27632 inhibited the invasion of rounded MDA-MB-435S cells in collagen I gels and did not modify the invasion of MDA-MB-231, cells with an elongated morphology. Focal adhesion formation, which is dependent on RhoA-ROCK activity, may limit tumor cell migration. For example, collagen I induces the activation of RhoA and focal adhesion formation in squamous carcinoma cells and treatment with Y27632 reduces the

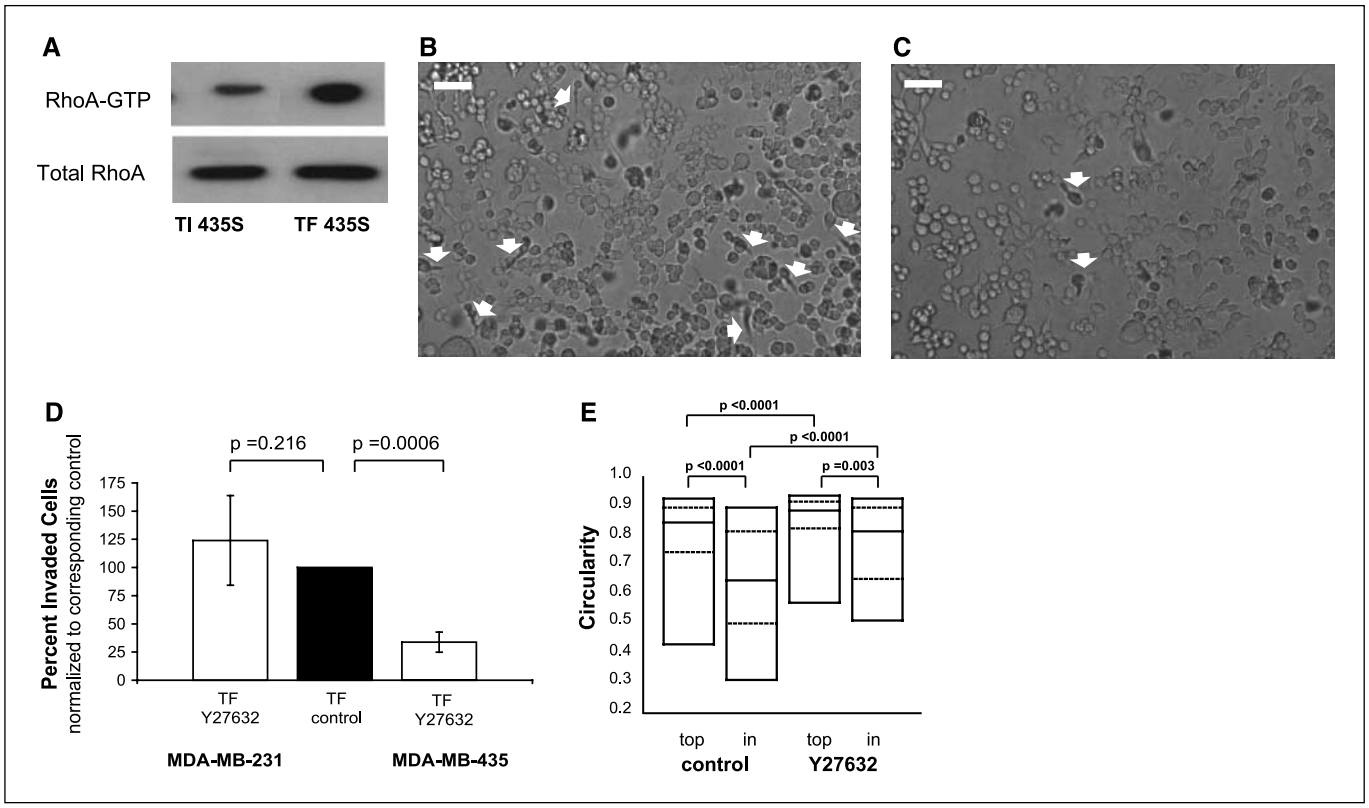

Figure 5. *A,* measurement of GTP-bound RhoA in pull-down assays showed a higher RhoA activity for MDA-MB-435S cells adhering to telopeptide-free (*TF*) than telopeptide-intact (*TI*) collagen I gels. Snapshot (10×) of control (*B*) and Y27632-treated (*C*) MDA-MB-435S cells on top and inside telopeptide-free gels, 4 days after seeding. Y27632 decreases the invasion and increases the circularity of the invaded cells (*arrows*). Bar, 50 μm. *D,* MDA-MB-231 and MDA-MB-435S cell invasion in telopeptide-free gels in the presence of Y27632 inhibitor as percentage of the corresponding invasion in untreated telopeptide-free gels. *Columns,* mean (n = 3); *bars,* SD. Y27632 significantly decreased the invasion of MDA-MB-435S cells but had no effect on the invasion of MDA-MB-231 cells. *E,* percentile plot of cell shape circularity on top and inside telopeptide-free collagen for MDA-MB-435S cells treated with the Rho/ROCK inhibitor Y27632 and corresponding control. The inhibitor significantly increased the cell circularity on top and inside the gel.

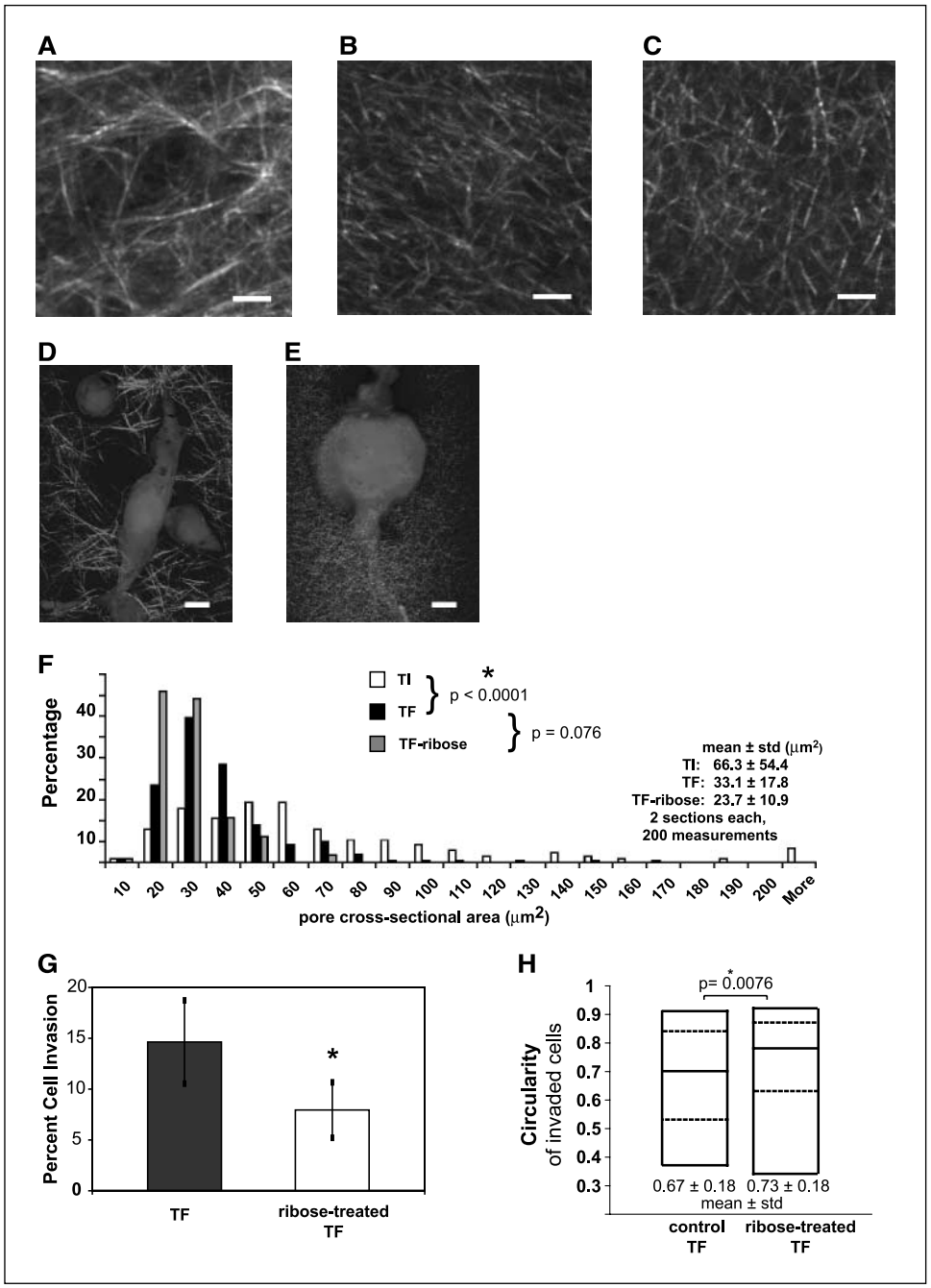

Figure 6. SHG optical sections (parallel to the surface of the gel) from a three-dimensional volume of a (*A*) telopeptide-intact (*TI*), (*B*) telopeptide-free (*TF*), and (*C*) telopeptide-free collagen gels after post-polymerization treatment with 100 mmol/L ribose for 5 days. Images were acquired with a 20× 0.9 NA lens and were contrast stretched to the same extent; a noise reduction filter was applied. The telopeptide-intact lattice is formed by thick, long fibers creating well-defined pores. The telopeptide-free lattice has shorter, thinner fibers and smaller pores. Ribose cross-links the collagen network with no effect on the lattice structure. Images (*D*) and (*E*) are composite images of SHG and calcein-stained MDA-MB-435S cells seeded in telopeptide-intact and telopeptide-free gels, respectively. These are single image sections from a three-dimensional volume, imaged just below the surface of the gels. Both images are from a 63× 0.9 NA lens and were contrast stretched to highlight the structure of the gel. *F,* distribution of the estimated pore cross-sectional area in telopeptide-intact and telopeptide-free collagen gels. The telopeptide-intact collagen lattice had significantly larger pore cross-sectional area and the lattice characteristics were similar for telopeptide-free and ribose-treated telopeptide-free gels. *G,* percent invasion of MDA-MB-435S cells in telopeptide-free and ribose-treated telopeptide-free gels. Ribose treatment increases the stiffness of telopeptide-free decreasing the invasion to 50%. *Columns,* mean (n = 3); *bars,* SD. *H,* cell shape circularity percentile plot for cells that invaded telopeptide-free and ribose-treated telopeptide-free collagen gels. Ribose treatment significantly increased the cell circularity.

formation of focal adhesions and enhances migration (46). Whereas the stiffness of collagen I can modulate RhoA activity (47), it is unclear if the differential activation of RhoA in MDA-MB-435S cells adhering to telopeptide-free and telopeptide-intact collagen is related to differences in mechanical properties, cellular adhesion (e.g., integrin activation), or an interaction between collagen stiffness and integrin activation.

This study addressed for the first time how collagen I gels polymerized with or without telopeptides modulate RhoA activity and the migration and invasion of breast tumor cells. The enhancement of RhoA-ROCK activity in MDA-MB-435S cells by telopeptide-free collagen I promoted the changes in cellular morphodynamics and the motility and invasion of this metastatic cell line. In the absence of efficient pericellular proteolysis, tumor cells may exploit their cell shape plasticity to overcome the matrix barrier capitalizing on structural defects in the tumor stroma.

Acknowledgments

Received 5/12/2004; revised 4/11/2005; accepted 4/21/2005.

Grant support: NIH R24 grant CA-85146, Susan G. Komen postdoctoral fellowship (Z. Demou), and Swiss National Research Funding Grant 107362 (J.Y. Perentes).

The costs of publication of this article were defrayed in part by the payment of page charges. This article must therefore be hereby marked *advertisement* in accordance with 18 U.S.C. Section 1734 solely to indicate this fact.

We thank Dr. David Birk for his helpful suggestions with the purification of collagen I from rat tail.

References

1. Liotta LA, Kohn EC. The microenvironment of the tumour-host interface. Nature 2001;17:375–9.
2. De Wever O, Mareel M. Role of tissue stroma in cancer cell invasion. J Pathol 2003;200:429–47.
3. Friedl P, Wolf K. Tumour-cell invasion and migration: diversity and escape mechanisms. Nat Rev Cancer 2003; 3:362–74.
4. Friedl P, Brocker EB. The biology of cell locomotion within three-dimensional extracellular matrix. Cell Mol Life Sci 2000;57:41–64.
5. Albo D, Rothman VL, Roberts DD, Tuszynski GP. Tumour cell thrombospondin-1 regulates tumour cell adhesion and invasion through the urokinase plasminogen activator receptor. Br J Cancer 2000;83:298–306.
6. Ntayi C, Lorimier S, Berthier-Vergnes O, Hornebeck W, Bernard P. Cumulative influence of matrix metalloproteinase-1 and -2 in the migration of melanoma cells within three-dimensional type I collagen lattices. Exp Cell Res 2001;270:110–8.
7. Ellerbroek SM, Wu YI, Overall CM, Stack MS. Functional interplay between type I collagen and cell surface matrix metalloproteinase activity. J Biol Chem 2001;276:24833–42.
8. Devreotes PN, Zigmond SH. Chemotaxis in eukaryotic cells: a focus on leukocytes and *Dictyostelium*. Annu Rev Cell Biol 1988;4:649–86.
9. Wolf K, Mazo I, Leung H, et al. Compensation mechanism in tumor cell migration: mesenchymal-amoeboid transition after blocking of pericellular proteolysis. J Cell Biol 2003;160:267–77.
10. Kuznetsova N, Leikin S. Does the triple helical domain of type I collagen encode molecular recognition and fiber assembly while telopeptides serve as catalytic domains? Effect of proteolytic cleavage on fibrillogenesis and on collagen-collagen interaction in fibers. J Biol Chem 1999;274:36083–8.
11. Eyre DR, Paz MA, Gallop PM. Cross-linking in collagen and elastin. Annu Rev Cell Biol 1984;53:717–48.
12. Kemp P, Bell E, Falco L, et al; 0 419 111 B1, assignee. Collagen compositions and methods of preparation thereof. European Patent 1995.
13. Sato K, Ebihara T, Adachi E, Kawashima S, Hattori S, Irie S. Possible involvement of aminotelopeptide in self-assembly and thermal stability of collagen I as revealed by its removal with proteases. J Biol Chem 2000;275: 25870–5.
14. Siegel RC, Pinnell SR, Martin GR. Cross-linking of collagen and elastin. Properties of lysyl oxidase. Biochemistry 1970;9:4486–92.
15. Siegel RC, Fu JC, Chang Y. Collagen cross-linking: the substrate specificity of lysyl oxidase. Adv Exp Med Biol 1976;74:438–46.
16. Ramaswamy S, Ross KN, Lander ES, Golub TR. A molecular signature of metastasis in primary solid tumors. Nat Genet 2003;33:49–54.
17. Hasebe T, Mukai K, Tsuda H, Ochiai A. New prognostic histological parameter of invasive ductal carcinoma of the breast: clinicopathological significance of fibrotic focus. Pathol Int 2000;50:263–72.
18. Kauppila S, Stenback F, Risteli J, Jukkola A, Risteli L. Aberrant type I and type III collagen gene expression in human breast cancer *in vivo*. J Pathol 1998;186:262–8.
19. Kauppila S, Bode MK, Stenback F, Risteli L, Risteli J. Cross-linked telopeptides of type I and III collagens in malignant ovarian tumours *in vivo*. Br J Cancer 1999; 81:654–61.
20. Peyrol S, Raccurt M, Gerard F, Gleyzal C, Grimaud JA, Sommer P. Lysyl oxidase gene expression in the stromal reaction to *in situ* and invasive ductal breast carcinoma. Am J Pathol 1997;150:497–507.
21. Okada Y, Gonoji Y, Naka K, et al. Matrix metalloproteinase 9 (92-kDa gelatinase/type IV collagenase) from HT 1080 human fibrosarcoma cells. Purification and activation of the precursor and enzymic properties. J Biol Chem 1992;267:21712–9.
22. Knauper V, Cowell S, Smith B, et al. The role of the C-terminal domain of human collagenase-3 (MMP-13) in the activation of procollagenase-3, substrate specificity, and tissue inhibitor of metalloproteinase interaction. J Biol Chem 1997;272:7608–16.
23. Shimada T, Nakamura H, Ohuchi E, et al. Characterization of a truncated recombinant form of human membrane type 3 matrix metalloproteinase. Eur J Biochem 1999;262:907–14.
24. Kafienah W, Bromme D, Buttle DJ, Croucher LJ, Hollander AP. Human cathepsin K cleaves native type I and II collagens at the N-terminal end of the triple helix. Biochem J 1998;331:727–32.
25. Atley LM, Mort JS, Lalumiere M, Eyre DR. Proteolysis of human bone collagen by cathepsin K: characterization of the cleavage sites generating by cross-linked N-telopeptide neoepitope. Bone 2000;26:241–7.
26. Maemura M, Iino Y, Yokoe T, et al. Serum concentration of pyridinoline cross-linked carboxyterminal telopeptide of type I collagen in patients with metastatic breast cancer. Oncol Rep 2000;7:1333–8.
27. Simojoki M, Santala M, Risteli J, Kauppila A. Carboxyterminal telopeptide of type I collagen (ICTP) in predicting prognosis in epithelial ovarian cancer. Gynecol Oncol 2001;82:110–5.
28. Keskikuru R, Bloigu R, Risteli J, Kataja V, Jukkola A. Elevated preoperative serum ICTP is a prognostic factor for overall and disease-free survival in breast cancer. Oncol Rep 2002;9:1323–7.
29. Girton TS, Oegema TR, Tranquillo RT. Exploiting glycation to stiffen and strengthen tissue equivalents for tissue engineering. J Biomed Mater Res 1999;46:87–92.
30. Sahai E, Marshall CJ. Differing modes of tumour cell invasion have distinct requirements for Rho/ROCK signalling and extracellular proteolysis. Nat Cell Biol 2003;5:711–9.
31. Burton K. An aperture-shifting light microscopic method for rapidly quantifying positions of cells in 3D matrices. Cytometry 2003;54:125–31.
32. Demou ZN, McIntire LV. Fully automated three-dimensional tracking of cancer cells in collagen gels: determination of motility phenotypes at the cellular level. Cancer Res 2002;62:5301–7.
33. Brown E, McKee T, diTomaso E, et al. Dynamic imaging of collagen and its modulation in tumors *in vivo* using second-harmonic generation. Nat Med 2003;9: 796–800.
34. Friedl P, Maaser K, Klein CE, Niggemann B, Krohne G, Zanker KS. Migration of highly aggressive MV3 melanoma cells in 3D collagen lattices results in local matrix reorganization and shedding of $\alpha 2$ and $\beta 1$ integrins and CD44. Cancer Res 1997;57:2061–70.
35. Wang N. Mechanical interactions among cytoskeletal filaments. Hypertension 1998;32:162–5.
36. Friedl P. Prespecification and plasticity: shifting mechanisms of cell migration. Curr Opin Cell Biol 2004;16:14–23.
37. Troup S, Njue C, Kliewer EV, et al. Reduced expression of the small leucine-rich proteoglycans, lumican, and decorin is associated with poor outcome in node-negative invasive breast cancer. Clin Cancer Res 2003;9:207–14.
38. Wolf K, Muller R, Borgmann S, Brocker EB, Friedl P. Amoeboid shape change and contact guidance: T-lymphocyte crawling through fibrillar collagen is independent of matrix remodeling by MMPs and other proteases. Blood 2003;102:3262–9.
39. Clark EA, Golub TR, Lander ES, Hynes RO. Genomic analysis of metastasis reveals an essential role for RhoC. Nature 2000;406:532–5.
40. Bouzahzah B, Albanese C, Ahmed F, et al. Rho family GTPases regulate mammary epithelium cell growth and metastasis through distinguishable pathways. Mol Med 2001;7:816–30.
41. Sahai E, Marshall CJ. RHO-GTPases and cancer. Nat Rev Cancer 2002;2:133–42.
42. Croft DR, Sahai E, Mavria G, et al. Conditional ROCK activation *in vivo* induces tumor cell dissemination and angiogenesis. Cancer Res 2004;64:8994–9001.
43. Somlyo AV, Bradshaw D, Ramos S, Murphy C, Myers CE, Somlyo AP. Rho-kinase inhibitor retards migration and *in vivo* dissemination of human prostate cancer cells. Biochem Biophys Res Commun 2000;269: 652–9.
44. Nakajima M, Hayashi K, Katayama K, et al. Wf-536 prevents tumor metastasis by inhibiting both tumor motility and angiogenic actions. Eur J Pharmacol 2003; 459:113–20.
45. De Wever O, Nguyen QD, Van Hoorde L, et al. Tenascin-C and SF/HGF produced by myofibroblasts *in vitro* provide convergent pro-invasive signals to human colon cancer cells through RhoA and Rac. FASEB J 2004;18:1016–8.
46. Zhou H, Kramer RH. Integrin engagement differentially modulates epithelial cell motility by RhoA/ROCK and PAK1. J Biol Chem 2005;280:10624–35.
47. Wozniak MA, Desai R, Solski PA, Der CJ, Keely PJ. ROCK-generated contractility regulates breast epithelial cell differentiation in response to the physical properties of a three-dimensional collagen matrix. J Cell Biol 2003; 163:583–95.

Lack of Telopeptides in Fibrillar Collagen I Promotes the Invasion of a Metastatic Breast Tumor Cell Line

Zoe N. Demou, Michael Awad, Trevor McKee, et al.

Cancer Res 2005;65:5674-5682.